Concomitant appearance of conductivity and superconductivity in (111) $LaAlO_3/SrTiO_3$ interface with metal capping

R. S. Bisht, M. Mograbi, P. K. Rout, G. Tuvia, and Y. Dagan*
School of Physics and Astronomy, Tel-Aviv University, Tel Aviv 6997801, Israel

Hyeok Yoon, A. G. Swartz, and H. Y. Hwang
Department of Applied Physics, Geballe Laboratory for Advanced Materials, Stanford University, 476 Lomita Mall, Stanford, California 94305, USA and Stanford Institute for Materials and Energy Sciences, SLAC National Accelerator Laboratory, Menlo Park, California 94025, USA

L. L. Li and R. Pentcheva
Department of Physics and Center for Nanointegration Duisburg-Essen (CENIDE), University of Duisburg-Essen, Lotharstrasse 1, D-47057 Duisburg, Germany

(Received 3 February 2021; accepted 22 March 2022; published 11 April 2022)

In epitaxial polar-oxide interfaces, conductivity sets in beyond a finite number of monolayers (ML). This threshold for conductivity is explained by accumulating sufficient electric potential to initiate charge transfer to the interface. Here we experimentally and theoretically study the $LaAlO_3/SrTiO_3$ (111) interface where a critical thickness t_c of nine epitaxial $LaAlO_3$ ML is required to turn the interface from insulating to conducting and even superconducting. We show that t_c decreases to 3 ML when depositing a cobalt overlayer (capping) and 6 ML for platinum capping. The latter result contrasts with the (001) interface, where platinum capping increases t_c beyond the bare interface. Our density functional theory calculations with a Hubbard U term confirm the observed threshold for conductivity for the bare and the metal-capped interfaces. Interestingly, conductivity appears concomitantly with superconductivity for metal/$LaAlO_3/SrTiO_3$ (111) interfaces, in contrast with the metal/$LaAlO_3/SrTiO_3$ (001) interfaces where conductivity appears without superconductivity. We attribute this dissimilarity to the different orbital polarization of e'_g for the (111) versus d_{xy} for the (001) interface.

DOI: 10.1103/PhysRevMaterials.6.044802

I. INTRODUCTION

The interface between $LaAlO_3$ and $SrTiO_3$ exhibits two-dimensional conductivity [1], superconductivity [2], magnetism [3–8], metal-insulator transition [9], tunable Rashba spin-orbit interaction [10,11], quantum Hall states [12,13], and one-dimensional conductivity [14,15]. While the $LaAlO_3/SrTiO_3$ (001) interface has received significant scientific attention, the (111) interface remains less explored.

The Ti atoms in $SrTiO_3$ form triangular layers along the [111] direction [16,17]. Due to the trigonal symmetry, the degeneracy of the t_{2g} manifold is lifted, splitting into a_{1g} and e'_g orbitals that might lead to topologically nontrivial states in $SrTiO_3$ quantum wells [18] or to exotic superconductivity [19].

While different scenarios for the formation of conductivity have been proposed at the (001) interface, e.g., for amorphous films [20–22], in epitaxial films four monolayers of $LaAlO_3$ are needed for the formation of a two-dimensional electron system (2DES) at the $LaAlO_3/SrTiO_3$ (001) interface [9]. For the (111) interface, the critical thickness for conductivity is nine monolayers (ML) [16].

Transport properties of the $LaAlO_3/SrTiO_3$ (111) interface indicate a sixfold symmetry [23]. The (111) 2DES also exhibits superconductivity [24], linked to spin-orbit interaction [25]. Notably, upon carrier depletion with negative gate voltage, superconductivity transitions into a Bose-insulating state [26]. This behavior contrasts with the (001) interface where a weaker insulating state is observed for negative gate biases [27,28].

For spin injection and low-voltage transistor applications, the barrier produced by the minimal four monolayers of $LaAlO_3$ required for conductivity at the bare (001) interface or by the nine monolayers at the (111) interface is relatively strong. First-principles calculations [29] and experimental studies of various metal capping on (001) interfaces (metal/$LaAlO_3/SrTiO_3$) [30,31] show that the critical thickness for the onset of conductivity, t_c, can be reduced relative to the bare interface and that t_c increases with the metal work function.

Here we study the problem of the critical thickness for conductivity for (111) interfaces both experimentally and theoretically. We have also expanded our experimental research to the superconducting properties of both (001) and (111)

*Corresponding author: yodagan@tauex.tau.ac.il

metal/$LaAlO_3$/$SrTiO_3$ interfaces. We find that upon capping the $LaAlO_3$/$SrTiO_3$ (111) interface with cobalt (Co) and platinum (Pt), t_c is reduced from t_c(bare)= 9 ML to t_c(Co) = 3 ML and t_c(Pt) = 6 ML. Furthermore, once the (111) interface becomes conducting, it also becomes superconducting at low temperatures. This contrasts with the (001) interface where t_c(Pt)>t_c(bare).

Concomitant density functional theory calculations with a Hubbard U term (DFT+U) confirm the reduction of the critical thickness upon metal capping and indicate that conductivity at the (111) interface arises due to bands with e'_g orbital polarization. We conjecture that these bands are also responsible for superconductivity. This is in contrast with the (001) interface where the d_{xy} and the d_{yz}, d_{xz} bands are split due to their different effective masses along the direction of the confining potential (z direction) [32]. Spin-orbit coupling mixes them together [33], resulting in a lower-energy, nonsuperconducting band and a higher-energy, mobile band, which is responsible for superconductivity [17,34].

II. METHODS

A. Experimental methods

Epitaxial $LaAlO_3$ films with different thicknesses were grown on Ti, and TiO_2 terminated, atomically smooth (111), and (001) $SrTiO_3$ substrates, respectively, at an oxygen pressure of 1×10^{-4} Torr and temperature 780 °C using pulsed laser deposition. The detailed growth conditions and characterizations can be found in Refs. [25,35]. The thickness was *in situ* monitored by reflection high-energy electron diffraction (RHEED) (see Supplemental Material, Fig. S1 [36]). The samples were then transferred to a metal deposition chamber (electron beam for the Co and Ag and sputtering or electron beam for the Pt) where they were preannealed for two minutes at 200 °C and at a pressure of 1×10^{-8} Torr to remove surface contaminants [37]. Metallic layers of ≈ 3 nm of platinum (Pt), silver (Ag), or cobalt (Co) were deposited at room temperature. For the cobalt, we used an additional 3 nm AlO_x to prevent oxidation. Wire bonding was used to connect to the sample electrically.

B. Theoretical modeling

Density functional theory (DFT) calculations were performed on thin $LaAlO_3$ films on (111)-oriented $SrTiO_3$, using the projector augmented wave (PAW) method [38] as implemented in the VASP code [39]. The generalized gradient approximation was used for the exchange-correlation functional, as parametrized by Perdew, Burke, and Ernzerhof [40]. Static correlation effects were considered within the DFT + U formalism [41], employing $U = 3$ eV for the Ti 3d orbitals, in line with previous work [42–44]. The $LaAlO_3$ thin films on $SrTiO_3$ (111) were modeled in the slab geometry with two symmetric surfaces to eliminate spurious electric fields. The $LaAlO_3$/$SrTiO_3$ (111) slabs contain 7 monolayers (ML) of $SrTiO_3$ (substrate) and 3–9 ML of $LaAlO_3$ on both sides of the substrate. Additionally, in order to assess the role of metallic contacts, a Pt and Co ML was added on top of the $LaAlO_3$ film. The modeled slabs contain ∼60 atoms for 3 ML $LaAlO_3$ and ∼120 atoms for 9 ML $LaAlO_3$, depending on surface termination and metal capping. The lateral lattice constant of the modeled $LaAlO_3$/$SrTiO_3$ (111) slabs was fixed to the $SrTiO_3$ substrate ($a = 3.905$ Å) in a ($\sqrt{2}a \times \sqrt{2}a$) lateral unit cell. A vacuum region of 15 Å was adopted to minimize the interaction between the slab and its periodic images. A cutoff energy of 600 eV was used to truncate the plane-wave expansion and a Γ-centered k-point mesh of 12 × 12 × 1 to sample the Brillouin zone (BZ). The atomic positions were fully optimized taking into account octahedral rotations and distortions until the forces on all atoms were less than 0.01 eV/Å and the change in total energy was less than 10^{-6} eV. Spin polarization was also considered in the DFT+U calculations to account for possible magnetic moments of the Ti 3d electrons and the metal-capping layer.

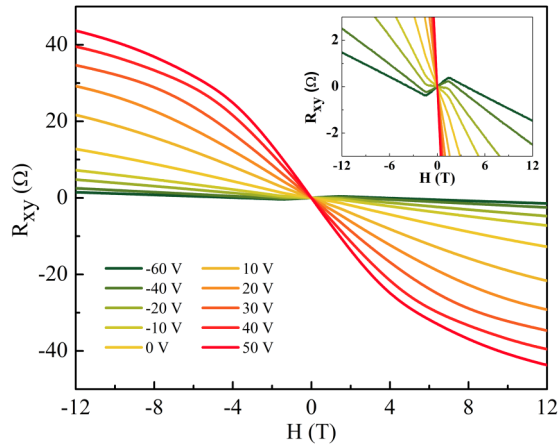

FIG. 1. Transverse resistance of AlO_x/Co/$LaAlO_3$/$SrTiO_3$ (111) for 4 ML $LaAlO_3$ as a function of a perpendicular magnetic field at different gate voltages at 2 K. The inset focuses on the negative gate voltage regime. The observed anomalous-Hall signal demonstrates the predominance of the Co layer properties in this regime. This is in contrast to the higher carrier density regime where the 2DES dominates.

III. RESULTS AND DISCUSSION

A. Experimental results

The transport measurements were performed on the samples with metal capping. In this configuration, the measured resistance is either a parallel combination of the metal-cap resistance and the 2DES at the conducting $LaAlO_3$/$SrTiO_3$ interface or only the metallic cap in the absence of 2DES. We demonstrate this by measuring the transverse resistance R_{xy}, i.e., the Hall signal of the AlO_x/Co/$LaAlO_3$/$SrTiO_3$ (111) interface for 4 $LaAlO_3$ ML, as shown in Fig. 1. While for positive gate voltage, the 2DES dominates and exhibits a signal resembling the $LaAlO_3$/$SrTiO_3$ (111) interface [25] when depleting the 2DES by negative gate voltage, the contribution of Co predominates as manifested in an anomalous-Hall signal, confirming the presence of two parallel channels for conduction. This behavior is similar to (001) with cobalt capping [31].

The transport studies conducted on the AlO_x/Co/$LaAlO_3$ /$SrTiO_3$ (111) interface show a reduction of the $LaAlO_3$ critical thickness for the onset of 2DES conductivity from

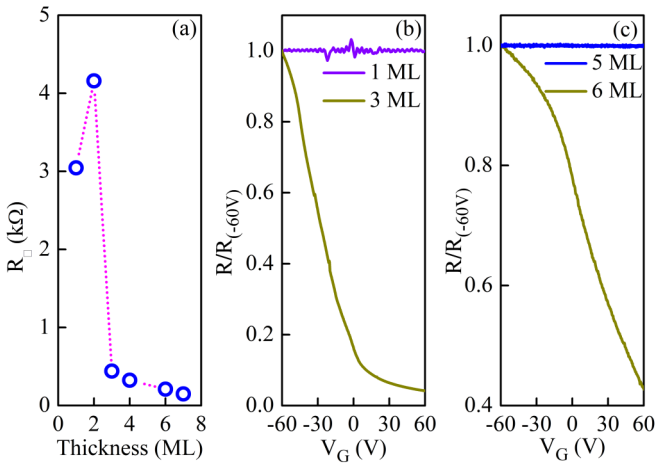

FIG. 2. (a) The sheet resistance ($R_{\square}$) of $AlO_x/Co/LaAlO_3/SrTiO_3$ (111) at 40 K as a function of $LaAlO_3$ thickness, where an abrupt drop in the resistance at 3 ML indicates that this is the critical thickness for the formation of 2DES at the $SrTiO_3/LaAlO_3$ interface. Note: The measured samples were not patterned; the geometrical factor for the sheet resistance calculation is within an error bar of ±10%. (b) The gate dependence of the normalized resistance ($R/R_{(-60V)}$) for $AlO_x/Co/LaAlO_3/SrTiO_3$ (111) with $LaAlO_3$ thickness of 1 and 3 monolayers. (c) The gate dependence of normalized resistance ($R/R_{(-60V)}$) for $Pt/LaAlO_3/SrTiO_3$ (111) for $LaAlO_3$ thickness of 5 and 6 monolayers.

9 $LaAlO_3$ ML (for the bare interface) to 3 ML (with Co capping). In Fig. 2(a), we show the sheet resistance of $AlO_x/Co/LaAlO_3/SrTiO_3$ (111) as a function of $LaAlO_3$ thickness at 40 K. For $LaAlO_3$ thickness below 3 ML, the resistance increases by nearly a factor of five. This indicates that 3 ML is the critical thickness of $LaAlO_3$ for the onset of conductivity with Co capping [t_c(Co) = 3 ML]. To verify that a 2DES is formed parallel to the metallic layer, we measured the resistance versus back-gate voltage. For a thin metallic layer parallel to a 2DES, one expects gate-dependent resistance due to the dominating contribution of 2DES. On the other hand, in the absence of a 2DES parallel to a metallic layer, we expect the gate dependence of the resistance to be immeasurably small due to the substantial carrier density in the metal. Figure 2(b) shows the gate dependence of $AlO_x/Co/LaAlO_3/SrTiO_3$ (111) for 1 and 3 $LaAlO_3$ ML. For the sample with a single $LaAlO_3$ ML, the normalized resistance ($R/R_{(-60V)}$) is flat as a function of gate voltage, suggesting the absence of 2DES at the $LaAlO_3/SrTiO_3$ interface. For 3 ML $LaAlO_3$, the data show a significant gate dependence, suggesting the formation of a 2DES at the $LaAlO_3/SrTiO_3$ (111) interface. We conclude that t_c becomes 3 ML upon Co capping for the (111) interface.

Previous studies on the metal-capped $LaAlO_3/SrTiO_3$ (001) interface show that t_c increases with the work function of the metal-capping layer [29]. To understand the role of the work function in (111) interfaces, we carried out experiments with Pt capping. The work function of platinum is generally higher than that of Co [45]. Surprisingly, we found that unlike the (001) interface, Pt capping reduces the critical thickness from t_c(bare) = 9 ML to t_c(Pt) = 6 ML. This is demonstrated in Fig. 2(c), where we show the gate dependence of $Pt/LaAlO_3/SrTiO_3$ (111) for 5 and 6 $LaAlO_3$ ML. The absence of gate dependence for 5 ML and the strong gate dependence for 6 ML suggests that t_c(Pt) = 6 ML. We interpret the saturation of the resistance at negative gate

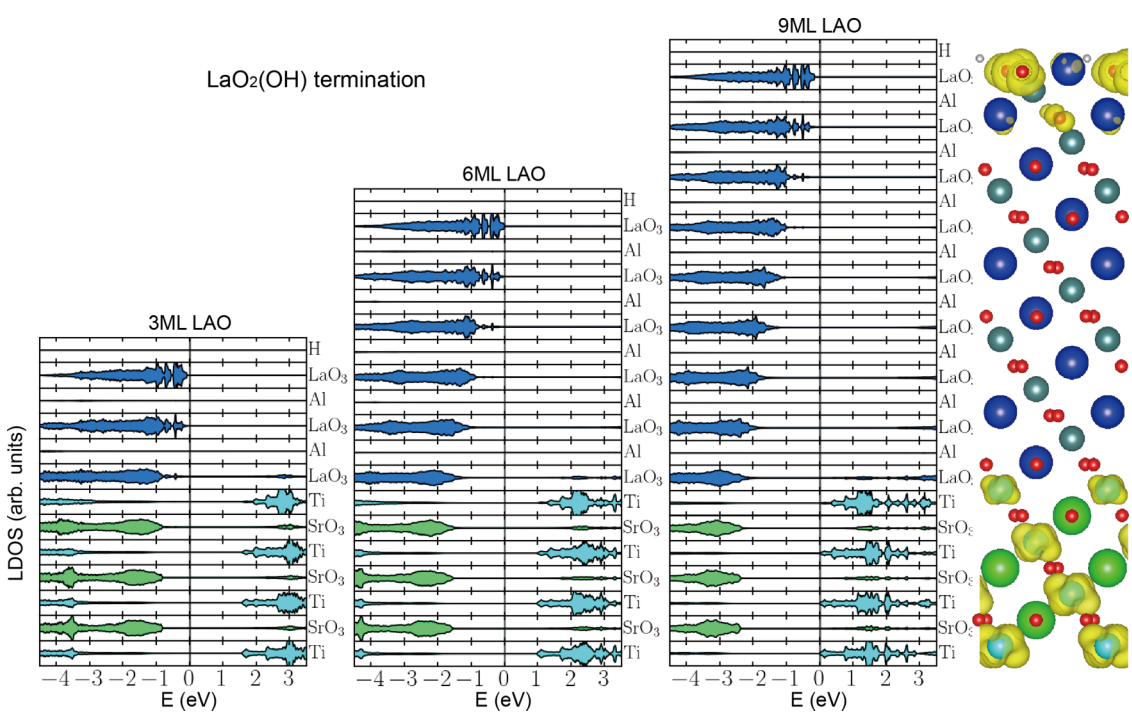

FIG. 3. Layer-resolved density of states (LDOS) of $LaAlO_3/SrTiO_3$ (111) slabs containing 7 ML of STO(111) and N ML of $LaAlO_3$ with a LaO_2(OH) termination (N = 3, 6, 9). A side view of half of the simulation cell and the electron density distribution integrated from −0.2 to the Fermi level for 9 ML LAO is shown in the right panel.

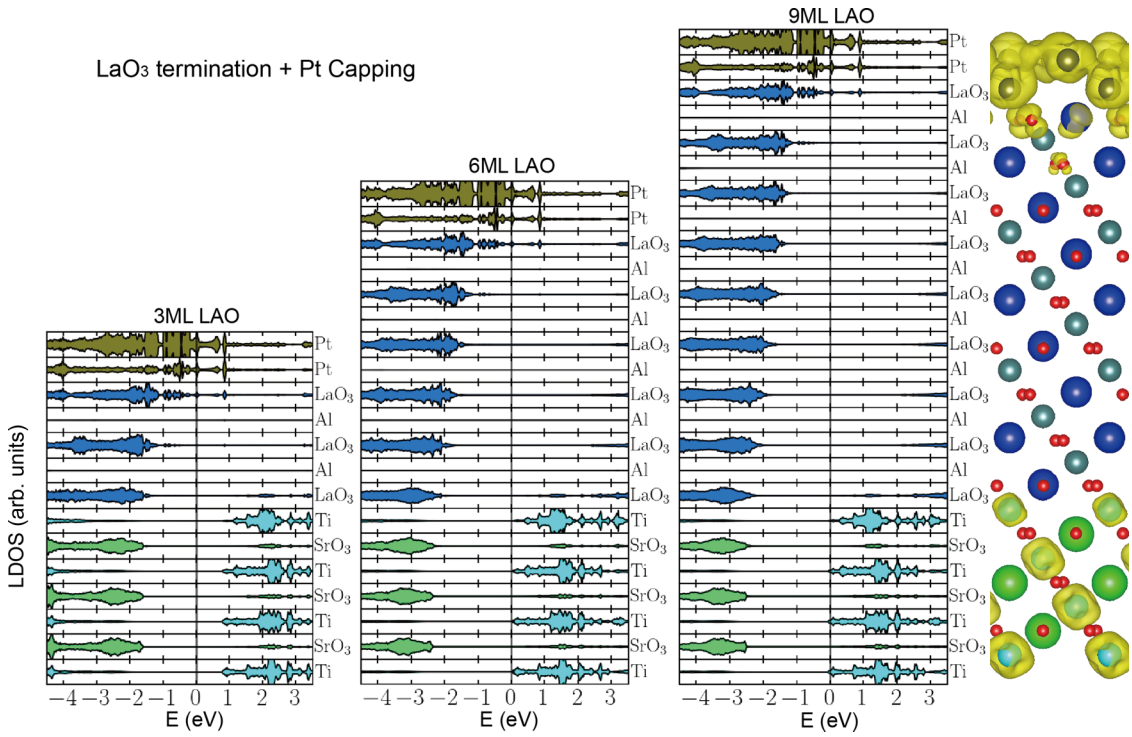

FIG. 4. Layer-resolved density of states (LDOS) of $LaAlO_3/SrTiO_3$ (111) slabs containing 7 ML of $SrTiO_3$ and N ML of $LaAlO_3$ capped with 1 ML of Pt ($N = 3, 6, 9$). A side view of half of the simulation cell and the electron density distribution integrated from -0.2 to the Fermi level for 9 ML $LaAlO_3$ with 1 ML Pt on top is shown in the far right panel.

voltage as a result of depletion of the 2DES and dominance of the metal-capping layer (see Fig. S2 in the Supplemental Material [36]). In Fig. S3(a) (Supplemental Material [36]), we also show the gate dependence of the extracted sheet resistance of 2DES for $AlO_x/Co/LaAlO_3/SrTiO_3$ (111) and $Pt/LaAlO_3/SrTiO_3$ (111) for 3 and 6 ML of $LaAlO_3$, respectively. We discuss the possibility of separating out the contribution of the 2DES from the combined resistance in the Supplemental Material [36]. In addition, in Fig. S3(b) [36], we show the sheet resistance of a pristine $LaAlO_3/SrTiO_3$ (111) film for 9 ML of $LaAlO_3$.

While suppression of t_c upon Co capping is observed for both the (111) and (001) $LaAlO_3/SrTiO_3$ interfaces, a reduction of t_c upon Pt capping occurs only for the (111) interface, whereas an increase in t_c is found for the Pt-capped (001) interface [31].

B. DFT+U results

In order to shed light on the origin of the experimentally observed critical thickness for an insulator-to-metal transition of the uncovered $LaAlO_3$ films on $SrTiO_3$ (111) as well as the role of metal capping, we have performed density functional theory calculations with a Hubbard U term. We considered different $LaAlO_3$ thicknesses and surface terminations, as well as metal capping using symmetric slabs with up to 130 atoms in the simulation cell. In the (111) direction, the perovskite structure comprises a stacking of AO_3-B layers. Taking into account the formal charges in these compounds, this leads to alternating $(SrO_3)^{4-}$ and Ti^{4+} layers in $SrTiO_3$ versus $(LaO_3)^{3-}$ and Al^{3+} layers in $LaAlO_3$. In analogy to the (001) interface, one expects a Ti termination of $SrTiO_3$ (111), on top of which $LaAlO_3$ is deposited. However, for an integer number of $LaAlO_3$ layers, the Al termination resulted in an opposite internal electric field within $LaAlO_3$ than the one known from the (001)-oriented films [46–48] with the valence-band maximum in the top layer pushed to lower energies. This is, however, fully consistent with the charges of the stacked layers along the [111] direction. Moreover, the system is metallic as the bottom of the Ti 3d band touches the Fermi level, independent of the $LaAlO_3$ thickness, thus showing no indication for an insulator-to-metal transition with $LaAlO_3$ thickness in contrast with the experimental observation. Therefore, this configuration was discarded. Next, we explored a LaO_3 termination: While this generates an internal electric field with the correct sign with an upward shift of the valence-band maximum in the $LaAlO_3$ layers as they approach the surface and a gradual reduction of the band gap with increasing $LaAlO_3$ thickness, it generates holes in the surface LaO_3 layer. As a result, the Ti 3d band at the interface is pushed to higher energies, leading to a higher critical thickness than the one observed in the experiment. This indicates that some kind of compensation of the holes in the surface LaO_3 layer is necessary. To simulate this effect, we have tried different concentrations of hydrogen (H) in the surface layer and identified that a $LaO_2(OH)$ termination with a single H on one out of three oxygens, as displayed in Fig. 3, provides the correct charge to suppress the surface holes and to induce the insulator-metal transition for t_c(bare) = 9 ML $LaAlO_3$ on $SrTiO_3$ (111), in agreement with experiment. We note that the compensation of the surface charge can also be achieved in other ways than hydroxylation, e.g., by creating

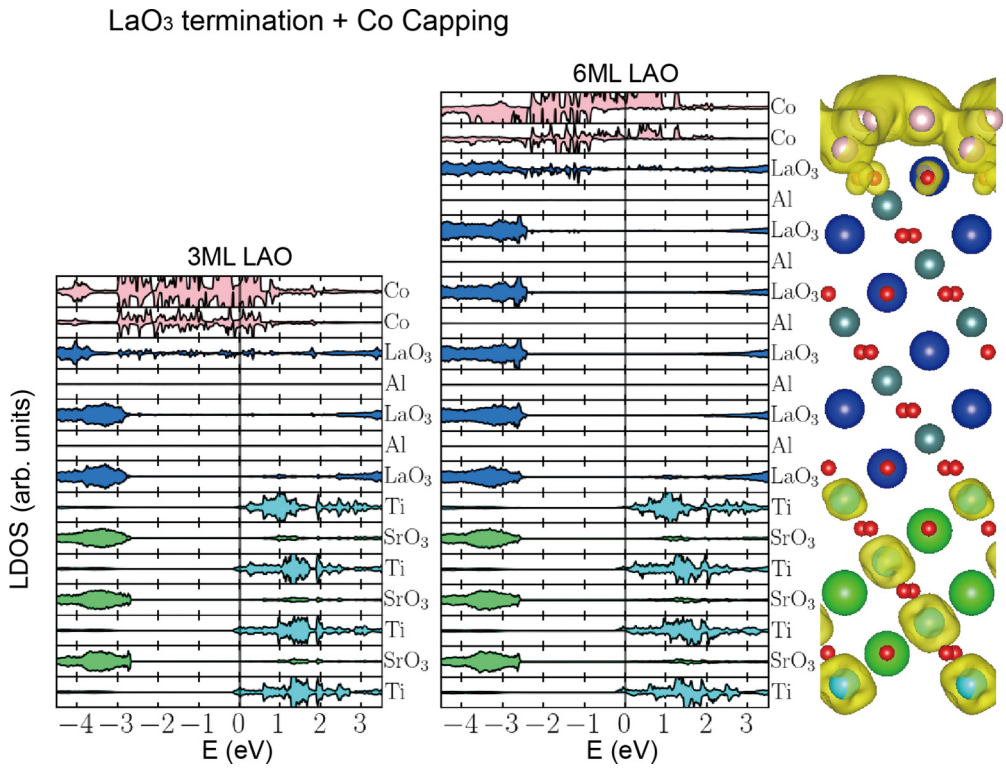

FIG. 5. The LDOS of $LaAlO_3/SrTiO_3$ (111) slabs containing seven monolayers of $SrTiO_3$ and three and six monolayers of $LaAlO_3$ capped with 1 ML of Co. A side view of half of the simulation cell and the electron density distribution integrated from −0.2 to the Fermi level for 6 ML $LaAlO_3$ with 1 ML Co on top is shown in the right panel.

half an oxygen vacancy per (1×1) surface cell. Surface vacancies were proposed as possible origin of the metal-to-insulator transition for the (001)-oriented case [49] and recently explored for the (111)-oriented interfaces [50]. Since the modeling of the correct concentration of surface vacancies requires a doubling of the already large unit cell, we continue the analysis with the LaO_3(OH) termination, which leads to the qualitatively correct critical thickness. As displayed in Fig. 3, the band gap of NLaAlO$_3$/SrTiO$_3$ (111) gradually decreases from 1.7 eV for 3 ML $LaAlO_3$ to 0.9 eV for 6 ML $LaAlO_3$ and is finally quenched for 9 ML $LaAlO_3$, consistent with the experimental observation. The experimental results presented above indicate that metal capping reduces t_c of $LaAlO_3/SrTiO_3$ (111). To assess the role of the metal capping, we covered the $LaAlO_3$ films with thicknesses of 3, 6, and 9 ML with Pt and Co. The calculated LDOS for a single monolayer of Pt and Co capping are displayed in Figs. 4 and 5, respectively. As can be seen, for the Pt capping, the Fermi level touches the conduction band at the LaO_3/Ti interface when the $LaAlO_3$ thickness reaches 6 ML, whereas for the Co capping, the insulator-metal transition already emerges at a $LaAlO_3$ thickness of 3 ML, consistent with the experimental observation. The 6 ML $LaAlO_3$ with Co capping represents the only case where a notable spin polarization of the 2DES is observed with magnetic moments of Ti ranging from 0.11 to 0.20 μ_B. To understand the observed critical thickness with metal capping, we list the calculated work functions of $LaAlO_3$ thin films on (111)$SrTiO_3$ for different $LaAlO_3$ thicknesses, surface terminations, surface hydrogenation, and metal capping in Table I. For comparison, the work function of free-standing Pt(111) and Co(111) slabs (7 ML thick) unstrained and strained at the lateral lattice constant of $SrTiO_3$ is also listed in Table I. We observe that the work function is weakly influenced by the $LaAlO_3$ thickness and is ∼5.0–5.2 eV for the LaO_3 termination and is reduced to ∼4.2–4.6 eV for the LaO_2(OH) termination. While the work function for the Co capping is ∼4.5–4.9 eV, it is significantly higher for the Pt capping (∼6.1 eV). This is consistent with the higher critical thickness of the latter

TABLE I. Calculated work functions (in eV) for different $LaAlO_3$ thicknesses (3, 6, and 9 ML), surface terminations (Al and LaO_3), partial surface hydrogenation [LaO_2(OH)], different metal cappings (Pt and Co), and freestanding Pt(111) and Co(111) slabs of 7 ML thickness unstrained and strained to the lateral lattice constant of $SrTiO_3$.

	3 ML	6 ML	9 ML
Al	4.478	4.599	4.534
LaO_3	5.153	5.042	5.146
LaO_2(OH)	4.186	4.193	4.631
LaO_3/Pt	6.080	6.076	6.072
LaO_3/Co	4.876	4.487	
	Pt(111)	Co(111)	
Free-standing	5.688	5.121	
Strained@a_{STO}	5.734	4.780	

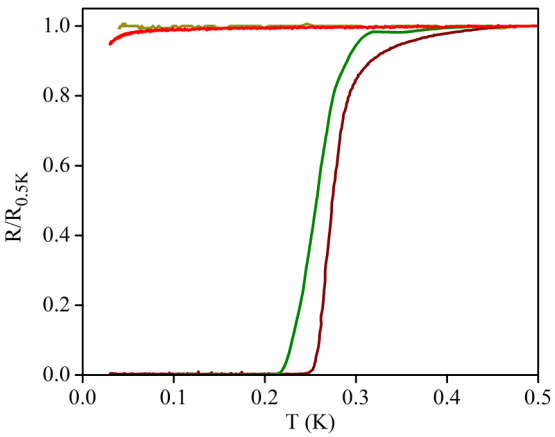

FIG. 6. The normalized resistance ($R/R_{(0.5K)}$) of AlO_x/Co/$LaAlO_3$ (3 ML)/$SrTiO_3$ (001) (dark yellow), Pt/$LaAlO_3$ (9 ML)/$SrTiO_3$ (001) (red), AlO_x/Co/$LaAlO_3$ (3 ML)/$SrTiO_3$ (111) (olive), and Pt/$LaAlO_3$ (6 ML)/$SrTiO_3$ (111) (wine). The $LaAlO_3$/$SrTiO_3$ (111) interfaces capped with Co and Pt show a superconducting transition and the corresponding critical thickness of $LaAlO_3$ is 3 and 6 monolayers, respectively.

capping. Nevertheless, the work function alone cannot account for the reduction of the critical thickness with respect to the uncovered $LaAlO_3$ film. On the other hand, a distinct behavior is observed from the layer-resolved DOS in Fig. 4 and 5 for the systems with Co and Pt capping. While for Co capping the internal electric field within $LaAlO_3$ is quenched, for Pt there is still a considerable internal electric field, albeit smaller than for the bare $LaAlO_3$ film. Thus the different critical thicknesses for Co and Pt can be rationalized by the the different size of *p*-type Schottky barriers that forms between $LaAlO_3$ and the metal contact: 2.5 eV (Co) vs 1 eV (Pt). In contrast, for the (001)-oriented interface, the *p*-type Schottky barriers were similar for a Co and Pt contact (∼2.3 eV) [29], leading to similar band diagrams despite the difference in work function.

The right panels in Figs. 3–5 also show the spatial distribution of the quasi-2DES within $LaAlO_3$/$SrTiO_3$ (111) with and without a metal-capping layer, integrated from −0.2 to the Fermi level. In all cases, the Ti 3*d* bands in the $SrTiO_3$ part host the 2DES. The characteristic shape of the electron clouds around the Ti positions indicates a predominant e_g' orbital polarization. We also note that for the systems covered by Pt or Co, a second conducting channel is present in the surface layer.

C. Metal-capping effect on superconducting properties

The DFT+U calculations presented above unveil the origin of the critical thickness for a metal-to-insulator transition in $LaAlO_3$/$SrTiO_3$ (111) and the role of metal capping. We now turn to study the effect of metal capping on superconductivity for the (001) and (111) interfaces. Surprisingly, we find that all the (111) samples, which show conductivity upon metal capping, also show superconductivity. In Table II, we summarize the properties of the (001) and (111) interfaces with various $LaAlO_3$ thickness and different metal capping. Figure 6 displays the normalized resistance ($R/R_{(0.5K)}$) as a function of temperature for different (001) and (111) interfaces at the critical thickness t_c with Co and Pt capping.

TABLE II. Summary of the different samples measured for various thickness of $LaAlO_3$ upon different metal capping and the corresponding nature of the interface. Note: For (001) interface, one monolayer corresponds to one unit cell. "Yes" in the superconductivity column means that the sample reached zero resistance at some gate voltage and "Partial" means that a drop in resistance is observed at low temperatures in some of the gate voltages without reaching zero resistance.

Interface	Metal layer	Thickness (ML)	Conducting	Superconducting
(111)	Co	1	No	No
(111)	Co	2	No	No
(111)	Co	3	Yes	Yes
(111)	Co	4	Yes	Yes
(111)	Co	6	Yes	Yes
(111)	Co	7	Yes	Yes
(111)	Pt	5	No	No
(111)	Pt	6	Yes	Yes
(111)	Pt	9	Yes	Yes
(111)	Pt	12	Yes	Yes
(001)	Co	2	Yes	No
(001)	Co	3	Yes	No
(001)	Pt	9	Yes	Partial
(001)	Ag	3	Yes	Partial
(111)	Bare	9	Yes	Yes
(001)	Bare	10	Yes	Yes

To make sure that the observed superconductivity is a two-dimensional (2D) interfacial effect and not a spurious one resulting from the metal deposition process, we studied the temperature dependence of the perpendicular and parallel critical fields. We show in the Supplemental Material [36] that they both follow the expected 2D Ginzburg-Landau temperature dependence (see Fig. S4). The resulting coherence length (ξ) and the superconducting effective layer thickness (d) are displayed in Fig. S5 [36].

In Fig. 7, we show the behavior of the critical temperature and critical fields as a function of gate voltage for the Co- and Pt-capped (111) interface. The dome-shaped gate dependence and the values of T_c, as well as the perpendicular ($H_\perp$) and the parallel ($H_\parallel$) critical fields, are similar to the bare $LaAlO_3$/$SrTiO_3$ (111) interface [17,25].

One may claim that the absence of superconductivity in the Co-capped $LaAlO_3$/$SrTiO_3$ (001) is due to the Co ferromagnetism. Indeed, as previously shown in Fig. 1, the Co layer shows an anomalous-Hall effect. However, for such a thin cobalt film, one expects the magnetic coupling to be short ranged with a negligible effect on the 2DES.

How can we understand the robustness of superconductivity in (111) interfaces? Previous experimental studies on $LaAlO_3$/$SrTiO_3$ (111) interfaces show that even at strong negative gate voltages, superconductivity remains intact [25,26]. On the theory side, the curvature of the Fermi contour changes quickly upon charge accumulation, and both the conducting and superconducting bands get an equal contribution from

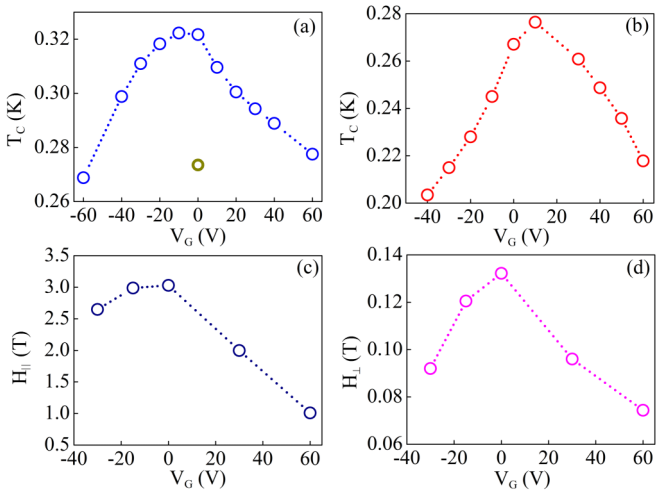

FIG. 7. (a) The critical temperature (T_c) of the Pt/$LaAlO_3$ (6 ML)/$SrTiO_3$ (111) interface; the dark-yellow circle shows the T_c of the as-cooled film. (b)–(d) The superconducting critical temperature, perpendicular critical field, and parallel critical field, respectively, of the AlO_x/Co/$LaAlO_3$ (3 ML)/$SrTiO_3$ (001) interface as a function of gate voltage. The values of these critical parameters are in good agreement with that of the uncapped interface. Note: T_c is defined as a temperature where the value of resistance drops by 50% of its value at 0.5 K.

the three degenerate t_{2g} orbitals [17]. By contrast, for the (001) interface, there is a distinct less mobile nonsuperconducting band and a mobile superconducting band due to the very different effective masses of the light d_{xy} and heavy d_{yz}, d_{xz} bands. It is possible that the interband repulsion [34] results in shifting the second band to higher energy, leaving only the metallic state. Our DFT+U calculations show that the e'_g bands lie lowest and contribute to conductivity at the (111) interfaces, suggesting that this type of band plays a significant role in the observed superconductivity.

IV. SUMMARY

Capping $LaAlO_3$/$SrTiO_3$ (111) by a metal reduces the critical thickness for the onset of conductivity from 9 ML for the bare interface to 6 and 3 ML for platinum and cobalt, respectively. DFT+U calculations are consistent with the experimental observations.

Importantly, all conducting (111) interfaces are also superconducting at low temperatures. This is in contrast with the (100) interfaces where conductivity emerges before superconductivity. The DFT+U results suggest that the different behavior of the superconducting state for the (111) and (100) interfaces with metal capping is related to the different orbital contribution to the 2DES: superconductivity takes place in the e'_g for the (111) interface, whereas for the (100) interface, the population of the heavy d_{xz}, d_{yz} bands is important for superconductivity.

Our findings suggest that proper choice of metal on top of the $LaAlO_3$ barrier can tune the barrier strength for various applications such as superconducting tunneling devices and ferromagnetic tunnel junction.

ACKNOWLEDGMENTS

We thank Moshe Goldstein and Udit Khanna for useful discussions. This research was supported by the Bi-national Science Foundation under Grant No. 2014047 and by the PAZI Foundation under Grant No. 326/21. R.P. and L.L.L. acknowledge computational time at the Leibniz Rechenzentrum, Project No. pr87ro. The work at SLAC/Stanford was supported by the U.S. Department of Energy, Office of Basic Energy Sciences, Division of Materials Sciences and Engineering, under Contract No. DE-AC02-76SF00515.

[1] A. Ohtomo and H. Y. Hwang, Nature (London) **427**, 423 (2004).
[2] N. Reyren, S. Thiel, A. D. Caviglia, L. F. Kourkoutis, G. Hammerl, C. Richter, C. W. Schneider, T. Kopp, A.-S. Rüetschi, D. Jaccard *et al.*, Science **317**, 1196 (2007).
[3] A. Brinkman, M. Huijben, M. van Zalk, J. Huijben, U. Zeitler, J. C. Maan, W. G. van der Wiel, G. Rijnders, D. H. A. Blank, and H. Hilgenkamp, Nat. Mater. **6**, 493 (2007).
[4] M. Sachs, D. Rakhmilevitch, M. Ben Shalom, S. Shefler, A. Palevski, and Y. Dagan, Physica C **470**, S746 (2010).
[5] J. A. Bert, B. Kalisky, C. Bell, M. Kim, Y. Hikita, H. Y. Hwang, and K. A. Moler, Nat. Phys. **7**, 767 (2011).
[6] A. Ron, E. Maniv, D. Graf, J.-H. Park, and Y. Dagan, Phys. Rev. Lett. **113**, 216801 (2014).
[7] S. Seri and L. Klein, Phys. Rev. B **80**, 180410(R) (2009).
[8] J.-S. Lee, Y. Xie, H. Sato, C. Bell, Y. Hikita, H. Hwang, and C.-C. Kao, Nat. Mater. **12**, 703 (2013).
[9] S. Thiel, G. Hammerl, A. Schmehl, C. W. Schneider, and J. Mannhart, Science **313**, 1942 (2006).
[10] M. Ben Shalom, M. Sachs, D. Rakhmilevitch, A. Palevski, and Y. Dagan, Phys. Rev. Lett. **104**, 126802 (2010).
[11] A. D. Caviglia, M. Gabay, S. Gariglio, N. Reyren, C. Cancellieri, and J.-M. Triscone, Phys. Rev. Lett. **104**, 126803 (2010).
[12] Y. Xie, C. Bell, M. Kim, H. Inoue, Y. Hikita, and H. Y. Hwang, Solid State Commun. **197**, 25 (2014).
[13] F. Trier, G. E. D. K. Prawiroatmodjo, Z. Zhong, D. V. Christensen, M. von Soosten, A. Bhowmik, Juan Maria Garcia Lastra, Y. Chen, T. S. Jespersen, and N. Pryds, Phys. Rev. Lett. **117**, 096804 (2016).
[14] A. Ron and Y. Dagan, Phys. Rev. Lett. **112**, 136801 (2014).
[15] M. Briggeman, M. Tomczyk, B. Tian, H. Lee, J.-W. Lee, Y. He, A. Tylan-Tyler, M. Huang, C.-B. Eom, D. Pekker *et al.*, Science **367**, 769 (2020).
[16] G. Herranz, F. Sánchez, N. Dix, M. Scigaj, and J. Fontcuberta, Sci. Rep. **2**, 758 (2012).
[17] U. Khanna, P. K. Rout, M. Mograbi, G. Tuvia, I. Leermakers, U. Zeitler, Y. Dagan, and M. Goldstein, Phys. Rev. Lett. **123**, 036805 (2019).
[18] D. Doennig, W. E. Pickett, and R. Pentcheva, Phys. Rev. Lett. **111**, 126804 (2013).

[19] M. S. Scheurer, D. F. Agterberg, and J. Schmalian, npj Quantum Mater. **2**, 9 (2017).
[20] M. P. Warusawithana, R. C., M. J. A., P. Roy, J. Ludwig, S. Paetel, T. Heeg, A. A. Pawlicki, L. F. Kourkoutis, M. Zheng *et al.*, Nat. Commun. **4**, 2351 (2013).
[21] S. W. Lee, Y. Liu, J. Heo, and R. G. Gordon, Nano Lett. **12**, 4775 (2012).
[22] Y. Chen, N. Pryds, J. E. Kleibeuker, G. Koster, J. Sun, E. Stamate, B. Shen, G. Rijnders, and S. Linderoth, Nano Lett. **11**, 3774 (2011).
[23] P. K. Rout, I. Agireen, E. Maniv, M. Goldstein, and Y. Dagan, Phys. Rev. B **95**, 241107(R) (2017).
[24] A. M. R. V. L. Monteiro, D. J. Groenendijk, I. Groen, J. de Bruijckere, R. Gaudenzi, H. S. J. van der Zant, and A. D. Caviglia, Phys. Rev. B **96**, 020504(R) (2017).
[25] P. K. Rout, E. Maniv, and Y. Dagan, Phys. Rev. Lett. **119**, 237002 (2017).
[26] M. Mograbi, E. Maniv, P. K. Rout, D. Graf, J.-H. Park, and Y. Dagan, Phys. Rev. B **99**, 094507 (2019).
[27] A. D. Caviglia, S. Gariglio, N. Reyren, D. Jaccard, T. Schneider, M. Gabay, S. Thiel, G. Hammerl, J. Mannhart, and J.-M. Triscone, Nature (London) **456**, 624 (2008).
[28] Z. Chen, A. G. Swartz, H. Yoon, H. Inoue, T. A. Merz, D. Lu, Y. Xie, H. Yuan, Y. Hikita, S. Raghu *et al.*, Nat. Commun. **9**, 1 (2018).
[29] R. Arras, V. G. Ruiz, W. E. Pickett, and R. Pentcheva, Phys. Rev. B **85**, 125404 (2012).
[30] E. Lesne, N. Reyren, D. Doennig, R. Mattana, H. Jaffrès, V. Cros, F. Petroff, F. Choueikani, P. Ohresser, R. Pentcheva *et al.*, Nat. Commun. **5**, 4291 (2014).
[31] D. C. Vaz, E. Lesne, A. Sander, H. Naganuma, E. Jacquet, J. Santamaria, A. Barthélémy, and M. Bibes, Adv. Mater. **29**, 1700486 (2017).
[32] A. F. Santander-Syro, O. Copie, T. Kondo, F. Fortuna, S. Pailhès, R. Weht, X. G. Qiu, F. Bertran, A. Nicolaou, A. Taleb-Ibrahimi *et al.*, Nature (London) **469**, 189 (2011).
[33] A. Joshua, S. Pecker, J. Ruhman, E. Altman, and S. Ilani, Nat. Commun. **3**, 1129 (2012).
[34] E. Maniv, M. B. Shalom, A. Ron, M. Mograbi, A. Palevski, M. Goldstein, and Y. Dagan, Nat. Commun. **6**, 8239 (2015).
[35] M. Ben Shalom, C. W. Tai, Y. Lereah, M. Sachs, E. Levy, D. Rakhmilevitch, A. Palevski, and Y. Dagan, Phys. Rev. B **80**, 140403(R) (2009).
[36] See Supplemental Material at http://link.aps.org/supplemental/10.1103/PhysRevMaterials.6.044802 for RHEED oscillations, resistance of 2DES without capping, analysis of critical field and measured coherence length, and role of Ag capping.
[37] H. Inoue, A. G. Swartz, N. J. Harmon, T. Tachikawa, Y. Hikita, M. E. Flatté, and H. Y. Hwang, Phys. Rev. X **5**, 041023 (2015).
[38] G. Kresse and D. Joubert, Phys. Rev. B **59**, 1758 (1999).
[39] G. Kresse and J. Furthmüller, Phys. Rev. B **54**, 11169 (1996).
[40] J. P. Perdew, K. Burke, and M. Ernzerhof, Phys. Rev. Lett. **77**, 3865 (1996).
[41] S. L. Dudarev, G. A. Botton, S. Y. Savrasov, C. J. Humphreys, and A. P. Sutton, Phys. Rev. B **57**, 1505 (1998).
[42] M. Nolan, S. D. Elliott, J. S. Mulley, R. A. Bennett, M. Basham, and P. Mulheran, Phys. Rev. B **77**, 235424 (2008).
[43] J. Betancourt, T. R. Paudel, E. Y. Tsymbal, and J. P. Velev, Phys. Rev. B **96**, 045113 (2017).
[44] B. Geisler, A. Blanca-Romero, and R. Pentcheva, Phys. Rev. B **95**, 125301 (2017).
[45] H. B. Michaelson, J. Appl. Phys. **48**, 4729 (1977).
[46] R. Pentcheva and W. E. Pickett, Phys. Rev. Lett. **102**, 107602 (2009).
[47] R. Pentcheva, M. Huijben, K. Otte, W. E. Pickett, J. E. Kleibeuker, J. Huijben, H. Boschker, D. Kockmann, W. Siemons, G. Koster, H. J. W. Zandvliet, G. Rijnders, D. H. A. Blank, H. Hilgenkamp, and A. Brinkman, Phys. Rev. Lett. **104**, 166804 (2010).
[48] G. Singh-Bhalla, P. B. Rossen, G. K. Pálsson, M. Mecklenburg, T. Orvis, S. Das, Y.-L. Tang, J. S. Suresha, D. Yi, A. Dasgupta, D. Doenning, V. G. Ruiz, A. K. Yadav, M. Trassin, J. T. Heron, C. S. Fadley, R. Pentcheva, J. Ravichandran, and R. Ramesh, Phys. Rev. Materials **2**, 112001(R) (2018).
[49] L. Yu and A. Zunger, Nat. Commun. **5**, 5118 (2014).
[50] T. Min, W. Choi, J. Seo, G. Han, K. Song, S. Ryu, H. Lee, J. Lee, K. Eom, C.-B. Eom *et al.*, Sci. Adv. **7**, eabe9053 (2021).